

MoMa: A Modular Deep Learning Framework for Material Property Prediction

Botian Wang^{*1,2} Yawen Ouyang^{*1} Yaohui Li^{*3} Yiqun Wang¹ Haorui Cui² Jianbing Zhang³
Xiaonan Wang⁴ Wei-Ying Ma¹ Hao Zhou¹

Abstract

Deep learning methods for material property prediction have been widely explored to advance materials discovery. However, the prevailing pre-train then fine-tune paradigm often fails to address the inherent diversity and disparity of material tasks. To overcome these challenges, we introduce MoMa, a **Modular** framework for **Materials** that first trains specialized modules across a wide range of tasks and then adaptively composes synergistic modules tailored to each downstream scenario. Evaluation across 17 datasets demonstrates the superiority of MoMa, with a substantial 14% average improvement over the strongest baseline. Few-shot and continual learning experiments further highlight MoMa’s potential for real-world applications. Pioneering a new paradigm of modular material learning, MoMa will be open-sourced to foster broader community collaboration.

1. Introduction

Accurate and efficient material property prediction is critical for accelerating materials discovery. Key properties such as formation energy and band gap are fundamental in identifying stable materials and functional semiconductors (Riebesell et al., 2023; Masood et al., 2023). While traditional approaches such as density functional theory (DFT) offer high precision (Jain et al., 2016), their prohibitive computational cost limits their practicality for large-scale screening (Fiedler et al., 2022; Lan et al., 2023).

Recently, deep learning methods have been developed to expedite traditional approaches (Xie & Grossman, 2018; Griesemer et al., 2023). Pre-trained force field models,

^{*}Equal contribution ¹Institute for AI Industry Research (AIR), Tsinghua University. This work was done during the internship of Yaohui and Haorui at AIR. ²Department of Computer Science and Technology, Tsinghua University ³School of Artificial Intelligence, National Key Laboratory for Novel Software Technology, Nanjing University ⁴Department of Chemical Engineering, Tsinghua University. Correspondence to: Hao Zhou <zhouhao@air.tsinghua.edu.cn>.

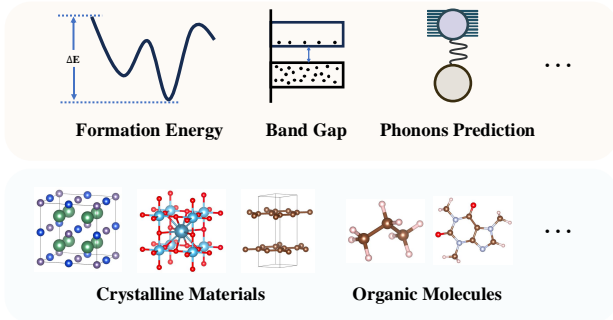


Figure 1: Illustration of the diversity of material properties (top) and systems (bottom). Note that material tasks are also disparate, with different laws governing the diverse properties and systems. These characteristics pose challenges for pre-training material property prediction models.

in particular, have shown remarkable success in generalizing to a wide spectrum of material property prediction tasks (Yang et al., 2024b; Barroso-Luque et al., 2024; Shoghi et al., 2023), outperforming specialized models trained from scratch. These models are typically pre-trained on the potential energy surface (PES) data of materials and then fine-tuned for the target downstream task.

Despite these advances, we identify two key challenges that undermine the effectiveness of current pre-training strategies for material property prediction: **diversity** and **disparity**.

First, material tasks exhibit significant diversity (Figure 1), which current pre-trained models fail to adequately cover. Existing models trained on PES-derived properties (e.g., force, energy, and stress) mostly focus on crystalline materials (Yang et al., 2024b; Barroso-Luque et al., 2024). However, material tasks span a wide variety of systems (e.g., crystals, organic molecules) and properties (e.g., thermal stability, electronic behavior, mechanical strength), making it difficult for methods trained on a limited set of data to generalize across the full spectrum of tasks.

Second, the disparate nature of material tasks presents huge obstacles for jointly pre-training a broad span of tasks. Material systems vary significantly in terms of bonding, atomic composition, and structural periodicity, while their properties are governed by distinct physical laws. For example,

mechanical strength in metals is primarily influenced by atomic bonding and crystal structure, whereas electronic properties like conductivity are determined by the material’s electronic structure and quantum mechanics. Consequently, training a single model across a wide range of tasks (Shoghi et al., 2023) may lead to knowledge conflicts, hindering the model’s ability to effectively adapt to downstream scenarios.

In this paper, we propose MoMa, a **Modular** deep learning framework for **Material** property prediction, to address the diversity and disparity challenge. To accommodate the **diversity** of material tasks, MoMa first trains on a multitude of high-resource property prediction datasets, centralizing them into transferrable modules. Furthermore, MoMa incorporates an adaptive composition algorithm that customizes support for diverse downstream scenarios. Recognizing the **disparity** among material tasks, MoMa encapsulates each task within a specialized module, eliminating task interference of joint training. In adapting MoMa to specific downstream tasks, its composition strategy adaptively integrates only the most synergistic modules, mitigating knowledge conflicts and promoting positive transfer.

Specifically, MoMa comprises two major stages: (1) *Module Training & Centralization*. Drawing inspiration from modular deep learning (Pfeiffer et al., 2023), MoMa trains dedicated modules for a broad range of material tasks, offering two versions: a full module for superior performance and a memory-efficient adapter module. These trained modules are centralized in MoMa Hub, a repository designed to facilitate knowledge reuse while preserving proprietary data for privacy-aware material learning. (2) *Adaptive Module Composition* (AMC). MoMa introduces the data-driven AMC algorithm that composes synergetic modules from MoMa Hub. AMC first estimates the performance of each module on the target task in a training-free manner, then heuristically optimizes their weighted combination. The resulting composed module is then fine-tuned for improved adaptation to the downstream task. Together, the two stages deliver a modular solution that enables MoMa to account for the diversity and disparity of material knowledge.

Empirical results across 17 downstream tasks showcase the superiority of MoMa, outperforming all baselines in **16/17** tasks, with an average improvement of **14%** compared to the second-best baseline. In **few-shot** settings, which are common in materials science, MoMa achieves even larger performance gains to the conventional pre-train then fine-tune paradigm. Additionally, we show that MoMa can expand its capability in **continual learning** settings by incorporating molecular tasks into MoMa Hub. The trained modules in MoMa Hub will be open-sourced, and we envision MoMa becoming a pivotal platform for the modularization and distribution of materials knowledge, fostering deeper community engagement to accelerate materials discovery.

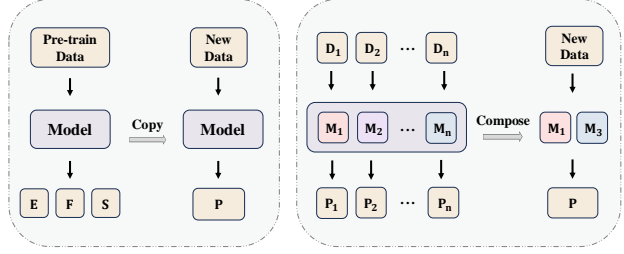


Figure 2: A comparison between the pre-train fine-tune paradigm and MoMa’s modular framework. (left): The prevailing scheme involves pre-training on force field data (with supervised prediction on energy, force, and stress), and then transfer to downstream tasks. (right): The modular learning scheme in MoMa trains and stores a broad spectrum of material tasks as modules, and adaptively composes them given a new material property prediction task.

2. Proposed Framework: MoMa

MoMa is a simple modular framework targeting the diversity and disparity of material tasks. The predominant pre-train then fine-tune strategy can only leverage a limited range of interrelated source tasks or indiscriminately consolidate conflicting knowledge into one model, resulting in suboptimal downstream performance. In contrast, the modular design of MoMa allows for the flexible and scalable integration of diverse material knowledge modules, and the effective and tailored adaptation to material property prediction tasks. Figure 2 illustrates this comparison.

2.1. Overview

MoMa involves two major stages: (1) training and centralizing modules into MoMa Hub; (2) adaptively composing these modules to support downstream material tasks.

In the first stage (Section 2.2), we encompass a wide range of material properties and systems into MoMa Hub. This accommodates the diversity of material tasks and addresses the task disparity by training specialized modules for each.

In the second stage (Section 2.3), we devise the Adaptive Module Composition algorithm. Given the downstream material task, the algorithm heuristically optimizes the optimal combination of module weights for MoMa Hub and composes a customized module based on the weights, which is subsequently fine-tuned on the task for better adaptation. Respecting the diverse and disparate nature of material tasks, our adaptive approach automatically discovers synergistic modules and excludes conflicting combinations by the data-driven assignment of module weights.

A visual overview of MoMa is provided in Figure 3.

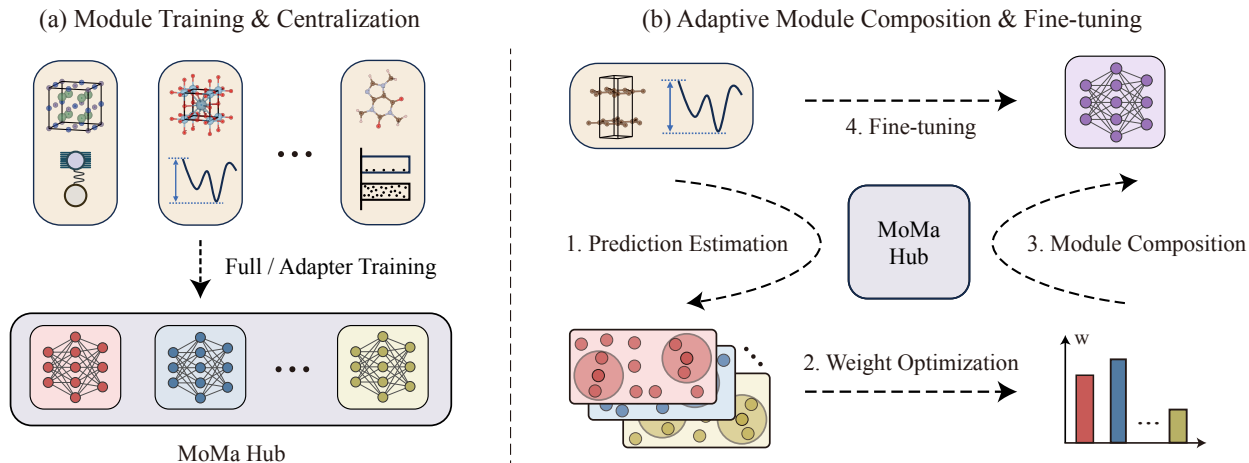


Figure 3: The MoMa framework. (a) During the Module Training & Centralization stage (Section 2.2), MoMa trains full and adapter modules for a wide spectrum of material tasks, constituting the MoMa Hub; (b) The Adaptive Module Composition (AMC) & Fine-tuning stage (Section 2.3) leverages the modules in MoMa Hub to compose a tailored module for each downstream task. The AMC algorithm comprises three steps: 1. module prediction estimation (with k NN); 2. module weight optimization; 3. module composition. The composed module is further fine-tuned on the task for better adaptation.

2.2. Module Training & Centralization

To better exploit the transferrable knowledge of open-source material property prediction datasets, we first train distinctive modules for each high-resource material task, and subsequently centralize these modules to constitute MoMa Hub.

Module Training Leveraging the power of state-of-the-art material property prediction models, we choose to employ a pre-trained backbone encoder f as the initialization for training each MoMa module. Note that MoMa is independent of the backbone model choice, which enables smooth integration with other pre-trained backbones.

We provide two parametrizations for the MoMa modules: the full module and the adapter module. For the full module, we directly treat each fully fine-tuned backbone as a module. The adapter module serves as a parameter-efficient variant where adapter layers (Houlsby et al., 2019) are inserted between each layer of the pre-trained backbone. The adapters are updated and the rest of the backbone is frozen. All of the adapters for each task are treated as one module. This implementation trade-offs the downstream performance in favor of a significantly lower GPU memory cost during training, which is particularly beneficial when the computational resources are constrained. When the training converges, we store the module parameters into a centralized repository \mathcal{H} termed MoMa Hub, formally:

$$\mathcal{H} = \{g_1, g_2, \dots, g_N\}, \quad g_i = \begin{cases} \theta_f^i & \text{(full module)} \\ \Delta_f^i & \text{(adapter module)} \end{cases}$$

where θ_f^i and Δ_f^i denote the full and adapter module param-

eters related to the i^{th} task and encoder f .

Module Centralization To support a wide array of downstream tasks, MoMa Hub needs to include modules trained on diverse material systems and properties. Currently, MoMa Hub encompasses 18 material property prediction tasks selected from the Matminer datasets (Ward et al., 2018) with over 10000 data points. These tasks span across a large range of material properties, including thermal properties (e.g. formation energy), electronic properties (e.g. band gap), mechanical properties (e.g. shear modulus), etc. For more details, please refer to Appendix B.1. To showcase the effect of scaling data diversity, we present the continual learning results in Section 3.5 after further incorporating molecular property prediction tasks into MoMa Hub. Note that MoMa is designed to be task-agnostic and may readily support a larger spectrum of tasks in the future.

An important benefit of the modular design of MoMa Hub is that it preserves proprietary data, which is prevalent in the field of materials, enabling privacy-aware contribution of new modules. Therefore, MoMa could serve as an open platform for the modularization of materials knowledge, which also facilitates downstream adaptation through a novel composition mechanism, as discussed in the following section.

2.3. Adaptive Module Composition & Fine-tuning

Given a labeled material property prediction dataset \mathcal{D} with m instances: $\mathcal{D} = \{(x_1, y_1), (x_2, y_2), \dots, (x_m, y_m)\}$, the second stage of MoMa customizes a task-specific model using the modules in MoMa Hub.

To achieve this, we devise the Adaptive Module Composition (AMC) algorithm. We highlight its key desiderata:

- **Selective:** Material tasks are inherently disparate. Hence only the most relevant modules shall be selected to avoid the negative interference of materials knowledge and encourage positive transfer to downstream tasks.
- **Data-driven:** As the diversity of tasks in MoMa Hub expands, it is impossible to rely solely on human expertise for module selection. A data-driven approach is required to mine the implicit relationships between the MoMa Hub modules and downstream tasks.
- **Efficient:** Enumerating all combinations of modules is impractical. Efficient algorithms shall be developed to return the optimal module composition using a reasonable amount of computational resources.

To meet these requirements, AMC is designed as a fast heuristic algorithm that first estimates the prediction of each module on the downstream task, then optimizes the module weights, and finally composes the selected modules to form the task-specific module. We now elaborate on the details of AMC, with its formal formulation in Algorithm 1.

Module Prediction Estimation We begin by estimating the predictive performance of each module in MoMa Hub \mathcal{H} on the downstream task \mathcal{D} . More accurate predictions indicate stronger relevance to the task and intuitively warrant higher weights in the composition.

For each module g_j in \mathcal{H} , we first take it to encode each input materials in the train set of task \mathcal{D} into a set of representation $\mathcal{X}^j = \{\mathbf{x}_1^j, \mathbf{x}_2^j, \dots, \mathbf{x}_m^j\}$ in which $\mathbf{x}_i^j = g_j(x_i)$. Then we obtain the estimated prediction of g_j on \mathcal{D} using a leave-one-out label propagation approach (Iscen et al., 2019). Specifically, we iteratively select one sample \mathbf{x}_i^j from \mathcal{X}^j and get the predicted label \hat{y}_i^j by calculating the weighted sum of its K nearest neighbors' labels within \mathcal{X}^j :

$$\hat{y}_i^j = \sum_{k=1}^K \frac{f_d(\mathbf{x}_i^j, \mathbf{x}_k^j)}{Z} y_k, \quad (1)$$

where \mathbf{x}_k^j denotes the k -th nearest neighbors of \mathbf{x}_i^j . The distance function f_d for calculating k NN is the exponential of cosine similarity between each pair of \mathbf{x}_i^j and \mathbf{x}_k^j . $Z = \sum_{k=1}^K f_d(\mathbf{x}_i^j, \mathbf{x}_k^j)$ is the normalizing term.

While other predictors are viable, we choose k NN due to its good trade-off in efficiency and accuracy. Also, its training-free nature enhances its flexibility in real-world scenarios, where the downstream data may be subject to updates.

Module Weight Optimization After estimating each module's prediction, we now have to select the optimal combination of modules tailored for the downstream task \mathcal{D} . To achieve this, the most straightforward approach is to compare the prediction error obtained after fine-tuning each combination of modules. However, this is infeasible due to the combinatorial explosion. Therefore, we reformulate the task as an optimization problem, using the prediction error before fine-tuning as a proxy metric (later referred to as *proxy error*). By optimizing the proxy error, we could obtain the optimal combination of weights.

Specifically, inspired by ensemble learning (Zhou et al., 2002; Zhou, 2016), we assign a weight w_j for each module g_j and calculate the output of the ensemble: $\sum_{j=1}^N w_j \hat{y}_i^j$. We then estimate the proxy error on the train set of \mathcal{D} for this weighted ensemble:

$$E_{\mathcal{D}} = \frac{1}{m} \sum_{i=1}^m \left(\sum_{j=1}^N w_j \hat{y}_i^j - y_i \right)^2 \quad (2)$$

To minimize the proxy error $E_{\mathcal{D}}$, we then utilize the open source cvxpy package (Diamond et al., 2014) to optimize the module weights. The objective is:

$$\underset{w_j}{\operatorname{argmin}} E_{\mathcal{D}}, \quad \text{s.t.} \quad \sum_{j=1}^N w_j = 1, w_j \geq 0 \quad (3)$$

Module Composition After the optimization converges, we can use the learned weights to compose a single customized module for the specific task.

Inspired by the recent success of model merging in NLP and CV (Wortsman et al., 2022; Ilharco et al., 2022; Yu et al., 2024; Li et al., 2024; Yang et al., 2024a), we adopt a simple yet surprisingly effective method by weighted averaging the parameters of the selected modules:

$$g_{\mathcal{D}} = \sum_{j=1}^N w_j^* g_j, \quad (4)$$

where w_j^* represents the optimized weight for the j -th module in Equation (3). Here, the weights underscore the relevance of each selected module to the downstream task.

While alternative composition methods, such as mixture-of-experts, are feasible, they incur high memory overhead as MoMa Hub expands, limiting their practical deployment under computational constraints. By contrast, our weighted-average composition uses fewer resources while effectively integrating knowledge from all modules. In the full-module setting, every module shares the same architecture and pre-trained backbone with identical initializations, providing a grounded foundation for successful knowledge composition (Zhou et al., 2024).

Table 1: **Main results for 17 material property prediction tasks.** The best MAE for each task is highlighted in **bold** and the second best result is underlined. Lower values indicate better performance. The results presented for each task are the average of five data splits, reported to three significant digits. For each method, the standard deviation of the test MAE across five random seeds is shown in parentheses. Additionally, the average rank and its standard deviation across the 17 datasets are provided to reflect the consistency of each method.

Datasets	CGCNN	MoE-(18)	JMP-MT	JMP-FT	MoMa (Adapter)	MoMa (Full)
Experimental Band Gap (eV)	0.471 (0.008)	0.374 (0.008)	0.377 (0.005)	<u>0.358</u> (0.014)	0.359 (0.009)	0.305 (0.006)
Formation Enthalpy (eV/atom)	0.193 (0.015)	<u>0.0949</u> (0.0016)	0.134 (0.001)	0.168 (0.007)	0.158 (0.009)	0.0839 (0.0013)
2D Dielectric Constant	2.90 (0.12)	2.29 (0.01)	<u>2.25</u> (0.06)	2.35 (0.07)	2.31 (0.04)	1.89 (0.03)
2D Formation Energy (eV/atom)	0.169 (0.006)	<u>0.106</u> (0.005)	0.140 (0.004)	0.125 (0.006)	0.112 (0.002)	0.0495 (0.0015)
Exfoliation Energy (meV/atom)	59.7 (1.5)	52.5 (0.8)	42.3 (0.5)	35.4 (2.0)	35.4 (0.9)	36.3 (0.2)
2D Band Gap (eV)	0.686 (0.034)	<u>0.532</u> (0.008)	0.546 (0.020)	0.582 (0.018)	0.552 (0.014)	0.375 (0.006)
3D Poly Electronic	32.5 (1.1)	27.7 (0.1)	23.9 (0.2)	<u>23.3</u> (0.3)	<u>23.3</u> (0.2)	23.0 (0.1)
3D Band Gap (eV)	0.492 (0.008)	0.361 (0.003)	0.423 (0.004)	0.249 (0.001)	<u>0.245</u> (0.002)	0.200 (0.001)
Refractive Index	0.0866 (0.0014)	0.0785 (0.0004)	0.0636 (0.0006)	0.0555 (0.0027)	<u>0.0533</u> (0.0023)	0.0523 (0.0010)
Elastic Anisotropy	3.65 (0.11)	3.01 (0.03)	<u>2.53</u> (0.26)	2.42 (0.36)	2.57 (0.61)	2.86 (0.28)
Electronic Dielectric Constant	0.168 (0.002)	0.157 (0.015)	0.137 (0.002)	0.108 (0.002)	<u>0.106</u> (0.002)	0.0885 (0.0048)
Dielectric Constant	0.258 (0.008)	0.236 (0.002)	0.224 (0.004)	0.171 (0.002)	<u>0.168</u> (0.002)	0.158 (0.002)
Phonons Mode Peak (cm ⁻¹)	0.127 (0.004)	0.0996 (0.0083)	0.0859 (0.0006)	0.0596 (0.0065)	<u>0.0568</u> (0.0009)	0.0484 (0.0026)
Poisson Ratio	0.0326 (0.0001)	0.0292 (0.0001)	0.0297 (0.0003)	0.0221 (0.0004)	<u>0.0220</u> (0.0003)	0.0204 (0.0002)
Poly Electronic	2.97 (0.10)	2.61 (0.13)	2.42 (0.03)	<u>2.11</u> (0.04)	2.13 (0.03)	2.09 (0.03)
Poly Total	6.54 (0.24)	5.51 (0.04)	5.52 (0.03)	<u>4.89</u> (0.06)	<u>4.89</u> (0.04)	4.86 (0.07)
Piezoelectric Modulus	0.232 (0.004)	0.208 (0.003)	0.199 (0.002)	<u>0.174</u> (0.004)	0.173 (0.003)	<u>0.174</u> (0.001)
Average Rank	6.00 (0.00)	4.12 (1.17)	3.94 (0.97)	2.88 (1.27)	<u>2.47</u> (0.94)	1.35 (0.86)

Downstream Fine-tuning To better adapt to the downstream task \mathcal{D} , the composed module $g_{\mathcal{D}}$ is appended with a task-specific head and then fine-tuned on \mathcal{D} to convergence.

3. Experiments

In this section, we conduct comprehensive experiments to demonstrate the empirical effectiveness of MoMa. The experimental setup is outlined in Section 3.1. The main results, discussed in Section 3.2, show that MoMa **substantially outperforms** baseline methods. Additionally, we conduct a thorough ablation study on the AMC algorithm as detailed in Section 3.3. Confronted with the data scarcity challenge common in real-world materials discovery settings, we evaluate MoMa’s few-shot learning ability in Section 3.4, where it achieves **even larger** performance gains compared to baselines. To further highlight the **flexibility and scalability** of MoMa, we extend MoMa Hub to include molecular datasets and present the continual learning results in Section 3.5. Finally, we visualize the module weights optimized by AMC in Section 3.6, highlighting MoMa’s potential for providing **valuable insights** into material properties.

3.1. Setup

Datasets To evaluate MoMa on material property prediction tasks, we conduct experiments on 17 tasks adhering to the benchmark settings established by Chang et al. (2022). Refer to Appendix B.1 for more details.

Implementation details For the pre-trained backbone of MoMa, we choose to employ the open-source JMP model (Shoghi et al., 2023) for representing material systems given its superior performance in property prediction tasks across both crystals and molecules. For the evaluation metric, we report the average mean absolute errors (MAE) across five random data splits to enhance the robustness of the results. Additional implementation details, including the network architecture, the hyper-parameters for MoMa, and the computational cost, are provided in Appendix B.2.

Baseline methods We compare the performance of MoMa with four baseline methods: CGCNN (Xie & Grossman, 2018), MoE-(18) (Chang et al., 2022), JMP-FT (Shoghi et al., 2023), and JMP-MT (Sanyal et al., 2018). CGCNN represents a classical method without pre-training. MoE-(18) trains separate CGCNN models for the upstream tasks of MoMa, then ensembles them as one model in a mixture-of-experts approach for downstream fine-tuning. JMP-FT directly fine-tunes the JMP pre-trained checkpoint on the downstream tasks. JMP-MT trains all tasks in MoMa with a multi-task pretraining scheme and then adapts to each downstream dataset with further fine-tuning. More discussions on baselines are included in Appendix B.3.

3.2. Main Results

Performance of MoMa As shown in Table 1, MoMa (Full) achieves the best performance with the lowest aver-

age rank of 1.35 and 14/17 best results. The adapter variant of MoMa follows, with an average rank of 2.47. Together, the two variants hold 16 out of 17 best results. They also exhibit the smallest rank deviations, indicating that MoMa consistently delivers reliable performance across tasks. Notably, MoMa (Full) outperforms JMP-FT in 14 tasks, with an impressive average improvement of 14.0%, highlighting the effectiveness of MoMa Hub modules in fostering material property prediction tasks. Moreover, MoMa (Full) surpasses JMP-MT in 16 out of 17 tasks with a substantial average margin of 24.8%, underscoring the advantage of MoMa in discovering synergistic knowledge modules.

Performance of baselines Among the baseline methods, JMP-FT performs the best with an average rank of 2.88, followed by JMP-MT with an average rank of 3.94. Though additionally trained on upstream tasks of MoMa Hub, JMP-MT still lags behind JMP-FT. We hypothesize that the inherent knowledge conflicts between the disparate material tasks pose a tremendous risk to the multi-task learning approach. We also observe that methods utilizing the JMP encoder outperform those based on CGCNN encoders. This demonstrates the good transferability of large force field models to material property prediction tasks.

3.3. Ablation Study of Adaptive Module Composition

Setup We conduct a fine-grained ablation study of the Adaptive Module Fusion algorithm. The following ablated variants are tested: (1) **Select average**, which discards the weights optimized in Equation (3) and applies arithmetic averaging for the selected modules; (2) **All average**, which simple averages all modules in MoMa Hub; (3) **Random selection**, which picks a random set of modules in MoMa Hub with the same module number as AMC. Further analysis experiments are done using the MoMa’s full parametrization, *i.e.*, MoMa (Full), due to its superior performance.

Results A visualization of the ablation results is presented in Figure 4. The ‘Select average’, ‘All average’, and ‘Random selection’ approaches perform worse to the main results using AMC in 13, 15, and 15 tasks, with an average increase of test MAE of 11.0%, 18.0%, and 20.2%. These results highlight the effectiveness of both the module selection and weighted composition strategies employed by AMC.

3.4. Performance in Few-shot Settings

Motivation & Setup To better assess the performance of MoMa in real-world materials discovery scenarios, where candidates with labeled properties are costly to acquire and often exceptionally scarce (Abed et al., 2024), we construct a few-shot learning setting and compare the performance of MoMa with JMP-FT, the strongest baseline method. For each downstream task, we randomly down-sample N data

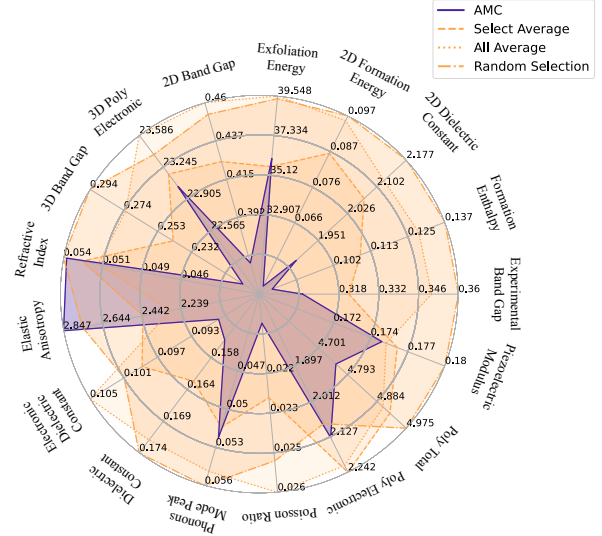


Figure 4: Ablation study of AMC. The main results using AMC (purple) are compared with the ablated variants (orange) that substitute AMC with select average, all average and random selection. The axis represents the MAE on each dataset and **smaller area is better**. The ablated results are inferior to the main results in 13, 15 and 15 out of 17 tasks.

points from the train set to construct the few-shot train set, on which we apply the AMC algorithm to compose modules from MoMa Hub. Then we perform downstream adaptation by fine-tuning on the N data points. The validation and test sets remain consistent with those in the standard settings to ensure a robust evaluation of model performance. Experiments are conducted with N set to 100 and 10, representing few-shot and extremely few-shot scenarios.

Results The average test losses for the 17 downstream tasks of MoMa compared to JMP-FT across the full-data, 100-data, and 10-data settings are illustrated in Figure 5. As expected, the test loss increases as the data size decreases, and MoMa consistently outperforms JMP-FT in all settings. Notably, the performance advantage of MoMa is more pronounced in the few-shot settings, with the normalized loss margin widening from 0.03 in the full-data setting to 0.11 and 0.15 in the 100-data and 10-data setting. This suggests that MoMa may offer even greater performance gains in real-world scenarios, where property labels are often limited, thereby hindering the effective fine-tuning of large pre-trained models. Complete results are shown in Table 4.

3.5. Continual Learning Experiments

Motivation & Setup Continual learning refers to the ability of an intelligent system to progressively improve by integrating new knowledge (Wang et al., 2024). We investigate this capability of MoMa by incorporating new modules

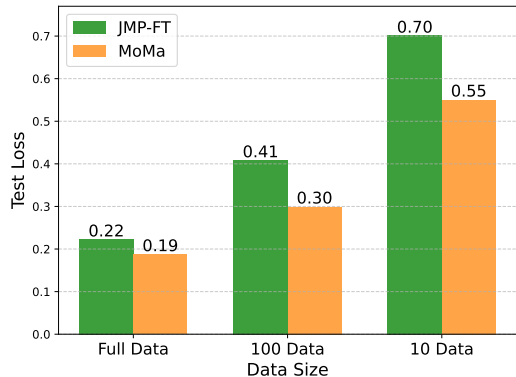


Figure 5: The average test losses of MoMa and JMP-FT across 17 downstream tasks under varying data availability settings. MoMa consistently outperforms JMP-FT in all settings. The loss reduction amplifies as the data size shrinks, highlighting the advantage of MoMa in few-shot settings. Results are averaged over five random data splits.

into MoMa Hub. Due to its modular nature, it is expected that MoMa will exhibit enhanced performance in tasks that are closely aligned with the new modules, while maintaining its performance when these additions are less relevant. We expand MoMa Hub to include the QM9 dataset (Ramakrishnan et al., 2014) and evaluate the results across the 17 benchmark material property prediction tasks. For more details on the setup, please refer to Appendix B.4.

Results We present the scatter plot of the reduction rate of test MAE w.r.t. the proxy error decrease in Figure 6 across datasets where QM9 modules are selected. We observe that: (1) The integration of QM9 modules leads to an average of 1.7% decrease in test set MAE; (2) a larger reduction in the AMC-optimized proxy error correlates with greater performance improvements post-fine-tuning (with a Pearson correlation of 0.69). We highlight the task of MP Phonons prediction, which marks a significant 11.8% decrease in test set MAE following the expansion of MoMa Hub.

3.6. Materials Insights Mining

Motivation We contend that the AMC weights derived in Equation (3) can offer interpretability for MoMa as well as provide valuable insights into material properties. To explore this, we interpret the weights as indicators for the relationships between MoMa Hub modules and downstream tasks. Following Chang et al. (2022), we present a log-normalized visualization of these weights in Figure 7.

Results We make several noteworthy observations:

- The weights assigned by AMC effectively capture physi-

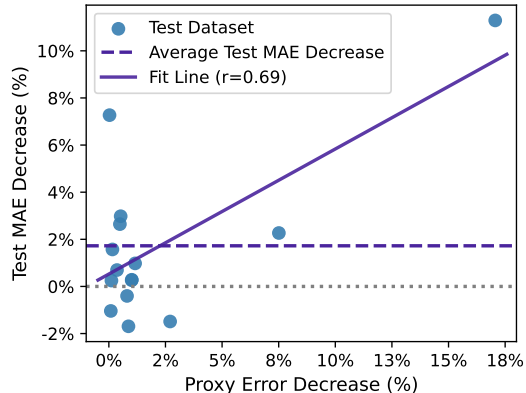


Figure 6: Scatter plot showing the relationship between the test MAE decrease and the proxy error (defined in Equation (3)) decrease after the addition of QM9 modules. The dashed line represents the average test MAE decrease. The solid line fits the results with linear regression.

cally intuitive relationships between material properties. For instance, the tasks of experimental band gap (row 1) and experimental formation energy (row 2) assign the highest weights to the computational band gap (columns 2 and 14) and formation energy modules (columns 1, 12, and 15). Also, for the task of predicting electronic dielectric constants, MoMa assigns high weights to the band gap modules, which is reasonable given the inverse relationship between the dielectric constant and the square of the band gap (Ravichandran et al., 2016).

- Some less-intuitive relationships also emerge. For the task of experimental band gap prediction (row 1), the formation energy module from the Materials Project (column 1) is assigned the second-highest weight. In the prediction of dielectric constant (row 9), modules related to thermoelectric and thermal properties (columns 5 and 6) are non-trivially weighted. However, the first-principles relationship between these tasks is indirect. We hypothesize that in addition to task relevance, other factors such as data distribution and size may also influence the weight assignments for AMC. Further investigation into these results are left to future work.

4. Related Work

4.1. Material Property Prediction with Deep Learning

Deep learning methods have been widely applied for predicting material properties (De Breuck et al., 2021). In a seminal work by Xie & Grossman (2018), CGCNN is designed to model crystalline materials with multi-edge graphs and leverage graph neural networks to learn crystal representations. Since then, a series of research (Choudhary &

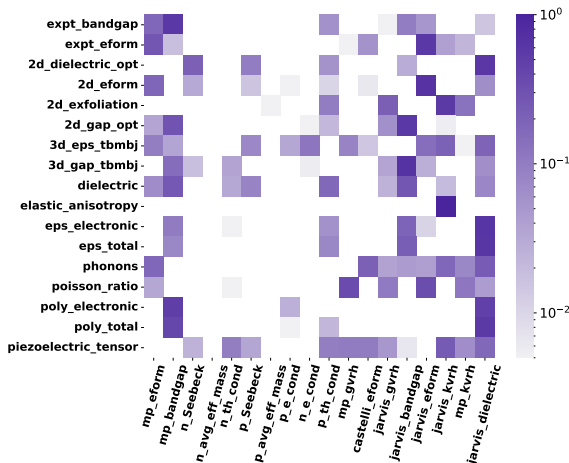


Figure 7: Heat map illustrating the AMC weights on one data split. The x-axis represents the task names of the MoMa Hub modules, while the y-axis shows the 17 material property prediction tasks in Table 1. Darker colors indicate higher weights, signifying a stronger correlation between the MoMa module and the downstream tasks.

DeCost, 2021; Yan et al., 2022; Das et al., 2023; Lin et al., 2023; Yan et al., 2024; Taniai et al., 2024) have focused on improving neural network architectures to better model the inductive biases of crystals for property prediction tasks.

Another line of work develops pre-training strategies to facilitate material property prediction (Jha et al., 2019; Magar et al., 2022; Zhang et al., 2023a; Wang et al., 2024; Song et al., 2024). Recently, a series of pre-trained force field models (Merchant et al., 2023; Batatia et al., 2023; Yang et al., 2024b; Neumann et al., 2024; Barroso-Luque et al., 2024) achieve remarkable accuracy in the stability prediction task of inorganic solid-state materials and show initial results in generalizing to a broader range of material properties. We highlight the JMP model proposed by Shoghi et al. (2023), which is trained on force and energy prediction tasks across multiple domains (small molecules, catalysts, etc.) and performs impressively when fine-tuned to downstream tasks of both molecules and crystals.

Extending beyond the prevailing pre-train and fine-tune paradigm, MoMa devises effective strategies to centralize material knowledge into modules and adaptively compose the modules to achieve superior downstream performance.

4.2. Modular Deep Learning

Modular deep learning (Pfeiffer et al., 2023) represents a promising paradigm in deep learning, where parameterized modules are composed, selected, and aggregated during the network training process. Different from the vanilla pre-train and fine-tune approach, modular methods employ

composable network architectures that enable more tailored adaptations to different tasks and domains. Notable examples of modular networks include mixture-of-experts (Jacobs et al., 1991; Shazeer et al., 2016), adapters (Houlsby et al., 2019) and LoRA (Hu et al., 2021). Recently, we have seen an increasing number of successful applications of modular deep learning across domains such as NLP and CV (Puigcerver et al., 2020; Pfeiffer et al., 2020; Huang et al., 2023; Zhang et al., 2023b; Tan et al., 2024; Pham et al., 2024), where its strengths in flexibility and minimizing negative interference have been demonstrated.

In the field of material property prediction, the idea of modular deep learning is still under-explored. A work most similar to MoMa is proposed by Chang et al. (2022). Their framework, termed MoE-(18), integrates 18 models trained on various source tasks with mixture of experts. MoMa distinguishes itself from MoE-(18) in two key aspects: (1) MoE-(18) loads all pre-trained models indiscriminately for each downstream task, whereas MoMa adaptively composes a subset of relevant modules to mitigate knowledge conflicts and encourage positive transfer. (2) MoE-(18) is designed to address the data scarcity issue and is limited to the mixture-of-experts approach, while MoMa introduces modularity to target the inherent challenges in materials science and is not restricted to any specific modular method. Hence, MoMa marks the first systematic effort to devise a modular deep learning framework for materials.

5. Conclusion & Outlook

In this paper, we present MoMa, a modular deep learning framework for material property prediction. Motivated by the challenges of diversity and disparity, MoMa first trains specialized modules across a wide spectrum of material tasks, constituting MoMa Hub. We then introduce the Adaptive Module Composition algorithm, which facilitates tailored adaptation from MoMa Hub to each downstream task by adaptively composing synergistic modules. Experimental results across 17 datasets demonstrate the superiority of MoMa, with few-shot and continual learning experiments further highlighting its data efficiency and scalability.

Finally, we discuss the prospects of MoMa in driving practical advancements in materials discovery. As an open-source platform enabling materials knowledge modularization and distribution, MoMa offers several key advantages: (1) secure, flexible upload of material modules to MoMa Hub without compromising proprietary data; (2) efficient customization of modules for downstream tasks; (3) enhanced property prediction accuracies, even in low-data scenarios. We envision MoMa facilitating a new paradigm of modular material learning and fostering broader community collaboration toward accelerated materials discovery.

Impact Statement

This paper presents work aimed at advancing the field of materials discovery through innovative machine learning techniques. The potential positive societal impacts include accelerating the discovery of new materials with desirable properties, benefiting industries such as energy, electronics, and manufacturing. However, there are risks associated with the mal-intended use of material knowledge to develop harmful or unsafe materials. To mitigate these risks, it is crucial to ensure that the application of this work adheres to ethical guidelines. While we do not foresee significant negative consequences in the near future, we recognize the importance of responsible usage and oversight in the application of these technologies.

References

- Abed, J., Kim, J., Shuaibi, M., Wander, B., Duijf, B., Mahesh, S., Lee, H., Gharakhanyan, V., Hoogland, S., Irtem, E., et al. Open catalyst experiments 2024 (ocx24): Bridging experiments and computational models. *arXiv preprint arXiv:2411.11783*, 2024.
- Barroso-Luque, L., Shuaibi, M., Fu, X., Wood, B. M., Dzamba, M., Gao, M., Rizvi, A., Zitnick, C. L., and Ulissi, Z. W. Open materials 2024 (omat24) inorganic materials dataset and models. *arXiv preprint arXiv:2410.12771*, 2024.
- Batatia, I., Benner, P., Chiang, Y., Elena, A. M., Kovács, D. P., Riebesell, J., Advincula, X. R., Asta, M., Avaylon, M., Baldwin, W. J., et al. A foundation model for atomistic materials chemistry. *arXiv preprint arXiv:2401.00096*, 2023.
- Castelli, I. E., Landis, D. D., Thygesen, K. S., Dahl, S., Chorkendorff, I., Jaramillo, T. F., and Jacobsen, K. W. New cubic perovskites for one-and two-photon water splitting using the computational materials repository. *Energy & Environmental Science*, 5(10):9034–9043, 2012.
- Chang, R., Wang, Y.-X., and Ertekin, E. Towards overcoming data scarcity in materials science: unifying models and datasets with a mixture of experts framework. *npj Computational Materials*, 8(1):242, 2022.
- Choudhary, K. and DeCost, B. Atomistic line graph neural network for improved materials property predictions. *npj Computational Materials*, 7(1):185, 2021.
- Choudhary, K., Kalish, I., Beams, R., and Tavazza, F. High-throughput identification and characterization of two-dimensional materials using density functional theory. *Scientific reports*, 7(1):5179, 2017.
- Choudhary, K., Cheon, G., Reed, E., and Tavazza, F. Elastic properties of bulk and low-dimensional materials using van der waals density functional. *Physical Review B*, 98(1):014107, 2018.
- Choudhary, K., Garrity, K. F., Reid, A. C., DeCost, B., Biacchi, A. J., Hight Walker, A. R., Trautt, Z., Hattrick-Simpers, J., Kusne, A. G., Centrone, A., et al. The joint automated repository for various integrated simulations (jarvis) for data-driven materials design. *npj computational materials*, 6(1):173, 2020.
- Das, K., Goyal, P., Lee, S.-C., Bhattacharjee, S., and Ganguly, N. Crysmmnet: multimodal representation for crystal property prediction. In *Uncertainty in Artificial Intelligence*, pp. 507–517. PMLR, 2023.
- De Breuck, P.-P., Hautier, G., and Rignanese, G.-M. Materials property prediction for limited datasets enabled by feature selection and joint learning with modnet. *npj computational materials*, 7(1):83, 2021.
- De Jong, M., Chen, W., Angsten, T., Jain, A., Notestine, R., Gamst, A., Sluiter, M., Krishna Ande, C., Van Der Zwaag, S., Plata, J. J., et al. Charting the complete elastic properties of inorganic crystalline compounds. *Scientific data*, 2(1):1–13, 2015a.
- De Jong, M., Chen, W., Geerlings, H., Asta, M., and Persson, K. A. A database to enable discovery and design of piezoelectric materials. *Scientific data*, 2(1):1–13, 2015b.
- Devlin, J. Bert: Pre-training of deep bidirectional transformers for language understanding. *arXiv preprint arXiv:1810.04805*, 2018.
- Diamond, S., Chu, E., and Boyd, S. CVXPY: A Python-embedded modeling language for convex optimization, version 0.2. <http://cvxpy.org/>, May 2014.
- Dunn, A., Wang, Q., Ganose, A., Dopp, D., and Jain, A. Benchmarking materials property prediction methods: the matbench test set and automatminer reference algorithm. *npj Computational Materials*, 6(1):138, 2020.
- Fiedler, L., Shah, K., Bussmann, M., and Cangi, A. Deep dive into machine learning density functional theory for materials science and chemistry. *Physical Review Materials*, 6(4):040301, 2022.
- Gasteiger, J., Shuaibi, M., Sriram, A., Günnemann, S., Ulissi, Z. W., Zitnick, C. L., and Das, A. Gemnet-oc: Developing graph neural networks for large and diverse molecular simulation datasets. *Transactions on Machine Learning Research*, 2022.
- Griesemer, S. D., Xia, Y., and Wolverton, C. Accelerating the prediction of stable materials with machine learning. *Nature Computational Science*, 3(11):934–945, 2023.

- Houlsby, N., Giurgiu, A., Jastrzebski, S., Morrone, B., De Laroussilhe, Q., Gesmundo, A., Attariyan, M., and Gelly, S. Parameter-efficient transfer learning for nlp. In *International conference on machine learning*, pp. 2790–2799. PMLR, 2019.
- Hu, E. J., Shen, Y., Wallis, P., Allen-Zhu, Z., Li, Y., Wang, S., Wang, L., and Chen, W. Lora: Low-rank adaptation of large language models. *arXiv preprint arXiv:2106.09685*, 2021.
- Huang, C., Liu, Q., Lin, B. Y., Pang, T., Du, C., and Lin, M. Lorahub: Efficient cross-task generalization via dynamic lora composition. *arXiv preprint arXiv:2307.13269*, 2023.
- Ilharco, G., Ribeiro, M. T., Wortsman, M., Gururangan, S., Schmidt, L., Hajishirzi, H., and Farhadi, A. Editing models with task arithmetic. *arXiv preprint arXiv:2212.04089*, 2022.
- Iscen, A., Tolias, G., Avrithis, Y., and Chum, O. Label propagation for deep semi-supervised learning. In *Proceedings of the IEEE/CVF conference on computer vision and pattern recognition*, pp. 5070–5079, 2019.
- Jacobs, R. A., Jordan, M. I., Nowlan, S. J., and Hinton, G. E. Adaptive mixtures of local experts. *Neural computation*, 3(1):79–87, 1991.
- Jain, A., Ong, S. P., Hautier, G., Chen, W., Richards, W. D., Dacek, S., Cholia, S., Gunter, D., Skinner, D., Ceder, G., et al. Commentary: The materials project: A materials genome approach to accelerating materials innovation. *APL materials*, 1(1), 2013.
- Jain, A., Shin, Y., and Persson, K. A. Computational predictions of energy materials using density functional theory. *Nature Reviews Materials*, 1(1):1–13, 2016.
- Jha, D., Choudhary, K., Tavazza, F., Liao, W.-k., Choudhary, A., Campbell, C., and Agrawal, A. Enhancing materials property prediction by leveraging computational and experimental data using deep transfer learning. *Nature communications*, 10(1):5316, 2019.
- Kim, G., Meschel, S., Nash, P., and Chen, W. Experimental formation enthalpies for intermetallic phases and other inorganic compounds. *Scientific data*, 4(1):1–11, 2017.
- Lan, J., Palizhati, A., Shuaibi, M., Wood, B. M., Wander, B., Das, A., Uyttendaele, M., Zitnick, C. L., and Ulissi, Z. W. Adsorbml: a leap in efficiency for adsorption energy calculations using generalizable machine learning potentials. *npj Computational Materials*, 9(1):172, 2023.
- Li, W., Gao, H.-a., Gao, M., Tian, B., Zhi, R., and Zhao, H. Training-free model merging for multi-target domain adaptation. *arXiv preprint arXiv:2407.13771*, 2024.
- Lin, Y., Yan, K., Luo, Y., Liu, Y., Qian, X., and Ji, S. Efficient approximations of complete interatomic potentials for crystal property prediction. In *International Conference on Machine Learning*, pp. 21260–21287. PMLR, 2023.
- Magar, R., Wang, Y., and Barati Farimani, A. Crystal twins: self-supervised learning for crystalline material property prediction. *npj Computational Materials*, 8(1):231, 2022.
- Masood, H., Sirojan, T., Toe, C. Y., Kumar, P. V., Haghshenas, Y., Sit, P. H., Amal, R., Sethu, V., and Teoh, W. Y. Enhancing prediction accuracy of physical band gaps in semiconductor materials. *Cell Reports Physical Science*, 4(9), 2023.
- Merchant, A., Batzner, S., Schoenholz, S. S., Aykol, M., Cheon, G., and Cubuk, E. D. Scaling deep learning for materials discovery. *Nature*, 624(7990):80–85, 2023.
- Neumann, M., Gin, J., Rhodes, B., Bennett, S., Li, Z., Choubisa, H., Hussey, A., and Godwin, J. Orb: A fast, scalable neural network potential. *arXiv preprint arXiv:2410.22570*, 2024.
- Petousis, I., Mrdjenovich, D., Ballouz, E., Liu, M., Winston, D., Chen, W., Graf, T., Schladt, T. D., Persson, K. A., and Prinz, F. B. High-throughput screening of inorganic compounds for the discovery of novel dielectric and optical materials. *Scientific data*, 4(1):1–12, 2017.
- Petretto, G., Dwaraknath, S., PC Miranda, H., Winston, D., Giantomassi, M., Van Setten, M. J., Gonze, X., Persson, K. A., Hautier, G., and Rignanese, G.-M. High-throughput density-functional perturbation theory phonons for inorganic materials. *Scientific data*, 5(1):1–12, 2018.
- Pfeiffer, J., Rücklé, A., Poth, C., Kamath, A., Vulić, I., Ruder, S., Cho, K., and Gurevych, I. Adapterhub: A framework for adapting transformers. *arXiv preprint arXiv:2007.07779*, 2020.
- Pfeiffer, J., Ruder, S., Vulić, I., and Ponti, E. M. Modular deep learning. *arXiv preprint arXiv:2302.11529*, 2023.
- Pham, C., Teterwak, P., Nelson, S., and Plummer, B. A. Mixturegrowth: Growing neural networks by recombining learned parameters. In *Proceedings of the IEEE/CVF Winter Conference on Applications of Computer Vision*, pp. 2800–2809, 2024.
- Puigcerver, J., Riquelme, C., Mustafa, B., Renggli, C., Pinto, A. S., Gelly, S., Keysers, D., and Houlsby, N. Scalable transfer learning with expert models. *arXiv preprint arXiv:2009.13239*, 2020.

- Ramakrishnan, R., Dral, P. O., Rupp, M., and Von Lilienfeld, O. A. Quantum chemistry structures and properties of 134 kilo molecules. *Scientific data*, 1(1):1–7, 2014.
- Ravichandran, R., Wang, A. X., and Wager, J. F. Solid state dielectric screening versus band gap trends and implications. *Optical materials*, 60:181–187, 2016.
- Ricci, F., Chen, W., Aydemir, U., Snyder, G. J., Rignanese, G.-M., Jain, A., and Hautier, G. An ab initio electronic transport database for inorganic materials. *Scientific data*, 4(1):1–13, 2017.
- Riebesell, J., Goodall, R. E., Jain, A., Benner, P., Persson, K. A., and Lee, A. A. Matbench discovery—an evaluation framework for machine learning crystal stability prediction. *arXiv preprint arXiv:2308.14920*, 2023.
- Ruddigkeit, L., Van Deursen, R., Blum, L. C., and Reymond, J.-L. Enumeration of 166 billion organic small molecules in the chemical universe database gdb-17. *Journal of chemical information and modeling*, 52(11):2864–2875, 2012.
- Sanyal, S., Balachandran, J., Yadati, N., Kumar, A., Rajagopalan, P., Sanyal, S., and Talukdar, P. Mt-cgcn: Integrating crystal graph convolutional neural network with multitask learning for material property prediction. *arXiv preprint arXiv:1811.05660*, 2018.
- Shazeer, N., Mirhoseini, A., Maziarz, K., Davis, A., Le, Q., Hinton, G., and Dean, J. Outrageously large neural networks: The sparsely-gated mixture-of-experts layer. In *International Conference on Learning Representations*, 2016.
- Shoghi, N., Kolluru, A., Kitchin, J. R., Ulissi, Z. W., Zitnick, C. L., and Wood, B. M. From molecules to materials: Pre-training large generalizable models for atomic property prediction. *arXiv preprint arXiv:2310.16802*, 2023.
- Song, Z., Meng, Z., and King, I. A diffusion-based pre-training framework for crystal property prediction. In *Proceedings of the AAAI Conference on Artificial Intelligence*, volume 38, pp. 8993–9001, 2024.
- Tan, S., Wu, D., and Monz, C. Neuron specialization: Leveraging intrinsic task modularity for multilingual machine translation. *arXiv preprint arXiv:2404.11201*, 2024.
- Taniai, T., Igarashi, R., Suzuki, Y., Chiba, N., Saito, K., Ushiku, Y., and Ono, K. Crystalformer: infinitely connected attention for periodic structure encoding. *arXiv preprint arXiv:2403.11686*, 2024.
- Wang, A., Kingsbury, R., McDermott, M., Horton, M., Jain, A., Ong, S. P., Dwaraknath, S., and Persson, K. A. A framework for quantifying uncertainty in dft energy corrections. *Scientific reports*, 11(1):15496, 2021.
- Wang, L., Zhang, X., Su, H., and Zhu, J. A comprehensive survey of continual learning: Theory, method and application. *IEEE Transactions on Pattern Analysis and Machine Intelligence*, 2024.
- Ward, L., Dunn, A., Faghaninia, A., Zimmermann, N. E., Bajaj, S., Wang, Q., Montoya, J., Chen, J., Bystrom, K., Dylla, M., et al. Matminer: An open source toolkit for materials data mining. *Computational Materials Science*, 152:60–69, 2018.
- Wortsman, M., Ilharco, G., Gadre, S. Y., Roelofs, R., Gontijo-Lopes, R., Morcos, A. S., Namkoong, H., Farhadi, A., Carmon, Y., Kornblith, S., et al. Model soups: averaging weights of multiple fine-tuned models improves accuracy without increasing inference time. In *International conference on machine learning*, pp. 23965–23998. PMLR, 2022.
- Xie, T. and Grossman, J. C. Crystal graph convolutional neural networks for an accurate and interpretable prediction of material properties. *Physical review letters*, 120(14):145301, 2018.
- Yan, K., Liu, Y., Lin, Y., and Ji, S. Periodic graph transformers for crystal material property prediction. *Advances in Neural Information Processing Systems*, 35:15066–15080, 2022.
- Yan, K., Fu, C., Qian, X., Qian, X., and Ji, S. Complete and efficient graph transformers for crystal material property prediction. *arXiv preprint arXiv:2403.11857*, 2024.
- Yang, E., Shen, L., Guo, G., Wang, X., Cao, X., Zhang, J., and Tao, D. Model merging in llms, mllms, and beyond: Methods, theories, applications and opportunities. *arXiv preprint arXiv:2408.07666*, 2024a.
- Yang, H., Hu, C., Zhou, Y., Liu, X., Shi, Y., Li, J., Li, G., Chen, Z., Chen, S., Zeni, C., et al. Mattersim: A deep learning atomistic model across elements, temperatures and pressures. *arXiv preprint arXiv:2405.04967*, 2024b.
- Yu, L., Yu, B., Yu, H., Huang, F., and Li, Y. Language models are super mario: Absorbing abilities from homol-ogous models as a free lunch. In *Forty-first International Conference on Machine Learning*, 2024.
- Zhang, D., Liu, X., Zhang, X., Zhang, C., Cai, C., Bi, H., Du, Y., Qin, X., Huang, J., Li, B., et al. Dpa-2: Towards a universal large atomic model for molecular and material simulation. *arXiv preprint arXiv:2312.15492*, 2023a.
- Zhang, J., Liu, J., He, J., et al. Composing parameter-efficient modules with arithmetic operation. *Advances in Neural Information Processing Systems*, 36:12589–12610, 2023b.

Zhou, Z., Chen, Z., Chen, Y., Zhang, B., and Yan, J. On the emergence of cross-task linearity in pretraining-finetuning paradigm. In *Forty-first International Conference on Machine Learning*, 2024.

Zhou, Z.-H. Learnware: on the future of machine learning. *Frontiers Comput. Sci.*, 10(4):589–590, 2016.

Zhou, Z.-H., Wu, J., and Tang, W. Ensembling neural networks: many could be better than all. *Artificial intelligence*, 137(1-2):239–263, 2002.

A. Algorithm for Adaptive Module Composition

The formal description of the Adaptive Module Composition algorithm is included in Algorithm 1.

Algorithm 1 Adaptive Module Composition

- 1: **Input:** MoMa Hub $\mathcal{H} = \{g_1, g_2, \dots, g_N\}$, Downstream Task \mathcal{D} .
 - 2: **Output:** adaptive module $g_{\mathcal{D}}$ for \mathcal{D} .
 - 3: **for** each module $g_j \in \mathcal{H}$ **do**
 - 4: Encode the input materials in the training set of \mathcal{D} using g_j to obtain $\mathcal{X}^j = \{\mathbf{x}_1^j, \mathbf{x}_2^j, \dots, \mathbf{x}_m^j\}$.
 - 5: **for** each sample $\mathbf{x}_i^j \in \mathcal{X}^j$ **do**
 - 6: Compute the predicted label \hat{y}_i^j for \mathbf{x}_i^j using k NN following Equation (1).
 - 7: **end for**
 - 8: **end for**
 - 9: Optimize the module weights w_j using cvxpy to minimize the proxy error defined in Equation (2), subject to:
 $\sum_{j=1}^N w_j = 1$ and $w_j \geq 0$. Denote the optimized weights for the j -th module as w_j^* .
 - 10: Compose the final adaptive module $g_{\mathcal{D}}$ by weighted averaging the parameters of the MoMa Hub modules:
 $g_{\mathcal{D}} = \sum_{j=1}^N w_j^* g_j$
 - 11: **Return:** The composed module $g_{\mathcal{D}}$.
-

B. Experimental Details

In this section, we provide more experimental details of MoMa regarding the datasets, implementation, baselines, and the continual learning setting.

B.1. Dataset Details

We primarily adopt the dataset setup proposed by Chang et al. (2022). Specifically, we select 35 datasets from Matminer (Ward et al., 2018) for our study, categorizing them into 18 high-resource material tasks, with sample sizes ranging from 10,000 to 132,000 (an average of 35,000 samples), and 17 low-data tasks, with sample sizes ranging from 522 to 8,043 (an average of 2,111 samples).

The high-resource tasks are utilized for training the MoMa Hub modules, as their larger data volumes are likely to encompass a wealth of transferrable material knowledge. A detailed introduction of these MoMa Hub datasets is included in Table 2.

The low-data tasks serve as downstream datasets to evaluate the effectiveness of MoMa and its baselines. This setup mimics real-world materials discovery scenarios, where downstream data are often scarce. To ensure robust and reliable comparison results, we exclude two downstream datasets with exceptionally small data sizes (fewer than 20 testing samples) from our experiments, as their limited data could lead to unreliable conclusions. A detailed introduction is included in Table 3.

Following Chang et al. (2022), all datasets are split into training, validation, and test sets with a ratio of 7:1.5:1.5. For the downstream low-data tasks, the splitting is performed randomly for 5 times to ensure the stability of evaluation.

B.2. Implementation Details of MoMa

Network Architecture We now introduce the network architecture of MoMa modules. The JMP (Shoghi et al., 2023) backbone is directly taken as the full module parametrization. JMP is pre-trained on ~ 120 million DFT-generated force-field data across large-scale datasets on catalyst and small molecules. JMP is a 6-layer GNN model with around 160M parameters which is based on the GemNet-OC architecture (Gasteiger et al., 2022). Note that MoMa is backbone-agnostic. JMP is selected due to its comprehensive strength across a wide range of molecular and crystal tasks, which allows us to seamlessly conduct the continual learning experiments. We leave the extrapolation of MoMa to other architectures as future work.

For the adapter module, we follow the standard implementation of adapter layers (Houlsby et al., 2019). Specifically, we insert adapter layers between each layer of the JMP backbone. Each layer consists of a downward projection to a bottleneck dimension and an upward projection back to the original dimension.

Table 2: Datasets for training MoMa Hub modules. **Num** stands for the number of samples in each dataset.

Datasets	Num	Description
MP E_f	132752	The energy change during the formation of a compound from its elements. Data from Jain et al. (2013).
MP E_g	106113	The PBE band gaps, calculated using the Perdew-Burke-Ernzerhof (PBE) functional, represent the energy difference between the valence and conduction bands in a material. Data from Jain et al. (2013).
MP G_{VRH}	10987	VRH-average shear modulus, an approximate value obtained by averaging the shear modulus of polycrystalline materials. Data from Jain et al. (2013).
MP K_{VRH}	10987	VRH-average bulk modulus, calculated by averaging the Voigt (upper bound) and Reuss (lower bound) bulk moduli. Data from Jain et al. (2013).
n-type σ_e	37390	n-type σ_e measures the material’s conductivity performance when electrons are the primary charge carriers. Data from Ricci et al. (2017).
p-type σ_e	37390	Similar to n-type σ_e , with holes as carriers. Data from Ricci et al. (2017).
n-type κ_e	37390	n-type κ_e evaluates the efficiency of n-type materials that can conduct both electricity and heat, which is crucial for understanding its performance in thermoelectric applications. Data from Ricci et al. (2017).
p-type κ_e	37390	Similar to n-type κ_e , with holes as carriers. Data from Ricci et al. (2017).
n-type S	37390	n-type S denotes the average conductivity eigenvalue, which measures thermoelectric conversion efficiency in the hole-conducting state when electrons act as the primary charge carriers. Data from Ricci et al. (2017).
p-type S	37390	Similar to n-type S , with holes as carriers. Data from Ricci et al. (2017).
n-type \bar{m}_e^*	21037	n-type \bar{m}_e^* denotes the average eigenvalue of conductivity effective mass, which measures the impact of the electron’s effective mass on the electrical conductivity. Data from Ricci et al. (2017).
p-type \bar{m}_e^*	20270	Similar to n-type \bar{m}_e^* , with holes as carriers. Data from Ricci et al. (2017).
Perovskite E_f	18928	Perovskite E_f refers to the heat of formation of perovskite, the amount of heat released or absorbed when the perovskite structure is formed from its constituent elements. Data from Castelli et al. (2012).
JARVIS E_f	25923	Formation energy from the JARVIS dataset (Choudhary et al., 2020).
JARVIS dielectric constant (Opt)	19027	Dielectric constant measures the material’s ability to polarize in response to an electric field in two-dimensional systems. Data from Choudhary et al. (2020).
JARVIS E_g	23455	PBE band gaps from the JARVIS dataset (Choudhary et al., 2020).
JARVIS G_{VRH}	10855	VRH-average shear modulus from the JARVIS dataset (Choudhary et al., 2020).
JARVIS K_{VRH}	11028	VRH-average bulk modulus from the JARVIS dataset (Choudhary et al., 2020).

Hyper-parameters For the training of JMP backbone, we mainly follow the hyper-parameter configurations in Shoghi et al. (2023), with slight modifications to the learning rate and batch size. During the module training stage of MoMa, we use a batch size of 64 and a learning rate of $5e-4$ for 80 epochs. During downstream fine-tuning, we adopt a batch size of 32 and a learning rate of $8e-5$. We set the training epoch as 60, with an early stopping patience of 10 epochs to prevent over-fitting. We adopt mean pooling of embedding for all properties since it performs significantly better than sum pooling in certain tasks (e.g. band gap prediction), which is consistent with findings in Shoghi et al. (2023).

For the adapter modules, we employ BERT-style initialization (Devlin, 2018), with the bottleneck dimension set to half of the input embedding dimension.

For the Adaptive Module Composition (AMC) algorithm, we set the number of nearest neighbors (K in Equation (1)) to 5. For the optimization problem formulated in Equation (3), we utilize the CPLEX optimizer from the cvxpy package (Diamond et al., 2014). AMC is applied separately for each random split of the downstream tasks to avoid data leakage.

Table 3: Downstream evaluation datasets.

Datasets	Num	Description
Experimental Band Gap (eV)	2481	The band gap of a material as measured through physical experiments. Data from Ward et al. (2018) .
Formation Enthalpy (eV/atom)	1709	The energy change for forming a compound from its elements, crucial for defining Gibbs energy of formation. Data from Wang et al. (2021) ; Kim et al. (2017) .
2D Dielectric Constant	522	The dielectric constant of 2D materials from Choudhary et al. (2017) .
2D Formation Energy (eV/atom)	633	The energy change associated with the formation of 2D materials from their constituent elements. Data from Choudhary et al. (2017) .
Exfoliation Energy (meV/atom)	636	The energy required to separate a single or few layers from bulk materials. Data from Choudhary et al. (2017) .
2D Band Gap (eV)	522	The band gap of 2D materials from Choudhary et al. (2017) .
3D Poly Electronic	8043	Poly electronic of 3D materials from Choudhary et al. (2018) .
3D Band Gap (eV)	7348	The band gap of 3D materials from Choudhary et al. (2018) .
Refractive Index	4764	The quantitative change of the speed of light as it passes through different media. Data from Dunn et al. (2020) ; Petousis et al. (2017) .
Elastic Anisotropy	1181	The directional dependence of a material’s elastic properties. Data from De Jong et al. (2015a) .
Electronic Dielectric Constant	1296	Electronic dielectric constant refers to the dielectric response caused by electronic polarization under an applied electric field. Data from Petretto et al. (2018) .
Dielectric Constant	1296	Dielectric constant of materials from Petretto et al. (2018) .
Phonons Mode Peak	1265	Phonon mode peak refers to the peak in the phonon spectrum caused by specific phonon modes. Data from Petretto et al. (2018) .
Poisson Ratio	1181	Poisson Ratio quantifies the ratio of transverse strain to axial strain in a material under uniaxial stress, reflecting its elastic deformation behavior. Data from De Jong et al. (2015a) .
Poly Electronic	1056	The Average eigenvalue of the dielectric tensor’s electronic component, where the dielectric tensor links a material’s internal and external fields. Data from Petousis et al. (2017) .
Poly Total	1056	The Average dielectric tensor eigenvalue. Data from Petousis et al. (2017) .
Piezoelectric Modulus	941	Piezoelectric modulus measures a material’s ability to convert mechanical stress into electric charge or vice versa. Data from De Jong et al. (2015b) .

Computational Cost Experiments are conducted on NVIDIA A100 80 GB GPUs. During the module training stage, training time ranges from 30 to 300 GPU hours, depending on the dataset size. While this training process is computationally expensive, it is a one-time investment, as the trained models are stored in MoMa Hub as reusable material knowledge modules. Downstream fine-tuning requires significantly less compute, ranging from 2 to 8 GPU hours based on the dataset scale. The full module and adapter module require similar training time; however, the adapter module greatly reduces memory consumption during training.

B.3. Baseline Details

The CGCNN baseline refers to fine-tuning the CGCNN model ([Xie & Grossman, 2018](#)) separately on 17 downstream tasks. Conversely, MoE-(18) involves training individual CGCNN models for each dataset in MoMa Hub and subsequently integrating these models using mixture-of-experts ([Jacobs et al., 1991](#); [Shazeer et al., 2016](#)). For the baseline results of CGCNN and MoE-(18), we adopt the open-source codebase provided by [Chang et al. \(2022\)](#) and follow the exactly same

Table 4: Test set MAE and average test loss of JMP-FT and MoMa under the full-data, 100-data, and 10-data settings. Results are averaged over five random data splits on one random seed. Results are preserved to the third significant digit.

Datasets	JMP-FT	MoMa	JMP-FT (100)	MoMa (100)	JMP-FT (10)	MoMa (10)
Experimental Band Gap	0.380	0.305	0.660	0.469	1.12	1.245
Formation Enthalpy	0.156	0.0821	0.273	0.101	0.514	0.143
2D Dielectric Constant	2.45	1.90	3.19	2.35	7.74	3.31
2D Formation Energy	0.135	0.0470	0.366	0.113	0.842	0.214
2D Exfoliation Energy	38.9	36.1	54.4	56.1	118	87.3
2D Band Gap	0.611	0.366	0.890	0.517	1.23	1.05
3D Poly Electronic	23.7	23.0	33.6	24.8	54.0	48.9
3D Band Gap	0.249	0.201	1.71	0.686	2.10	1.47
Dielectric Constant	0.0552	0.0535	0.134	0.102	0.289	0.231
Elastic Anisotropy	2.11	2.85	4.85	3.79	4.02	5.26
Electronic Dielectric Constant	0.108	0.0903	0.260	0.178	0.568	0.500
Total Dielectric Constant	0.172	0.155	0.361	0.287	0.543	0.527
Phonons Mode Peak	0.0710	0.0521	0.221	0.199	0.493	0.485
Poisson Ratio	0.0221	0.0203	0.0345	0.0317	0.0466	0.057
Poly Electronic	2.10	2.13	3.24	2.88	6.08	5.10
Total Poly	4.83	4.76	6.54	6.32	11.2	10.1
Piezoelectric Modulus	0.169	0.175	0.248	0.258	0.303	0.290
Average Test Loss	0.222	0.187	0.408	0.299	0.700	0.550

parameters as reported in their papers for the result duplication.

For JMP-FT, we use the JMP (large) checkpoint from the codebase open-sourced by [Shoghi et al. \(2023\)](#) and fine-tune it directly on the downstream tasks with a batch size of 64. JMP-MT adopts a multi-task pre-training strategy, training on all 18 MoMa Hub source tasks without addressing the conflicts between disparate material tasks. Starting from the same pre-trained checkpoint as JMP-FT, JMP-MT employs proportional task sampling and trains for 5 epochs across all tasks with a batch size of 16. The convergence of multi-task pre-training is indicated by a lack of further decrease in validation error on most tasks after 5 epochs. For downstream fine-tuning, both JMP-FT and JMP-MT adopt the same training scheme as the fine-tuning stage in MoMa.

B.4. Details on Continual Learning Experiments

The QM9 dataset ([Ramakrishnan et al., 2014](#)) comprises 12 quantum chemical properties (including geometric, electronic, energetic, and thermodynamic properties) for 134,000 stable small organic molecules composed of CHONF atoms, drawn from the GDB-17 database ([Ruddigkeit et al., 2012](#)). It is widely served as a comprehensive benchmarking dataset for prediction methods of the structure-property relationships in small organic molecules.

In the continual learning experiments, we expand the MoMa hub by including modules trained on the QM9 dataset. For module training, we adopt the same training scheme as the original MoMa modules, with the exception of using sum pooling instead of mean pooling, as it has been empirically shown to perform better ([Shoghi et al., 2023](#)).

C. More Experimental Results

We report the complete few-shot learning results in Table 4.